Chemistry & Biology
Article

Ligand-Interaction Kinetics of the Pheromone-Binding Protein from the Gypsy Moth, *L. dispar*: Insights into the Mechanism of Binding and Release

Yongmei Gong,[1] Tamara C.S. Pace,[2] Carlos Castillo,[1] Cornelia Bohne,[2] Melanie A. O'Neill,[1] and Erika Plettner[1,*]
[1]Department of Chemistry, Simon Fraser University, Burnaby, BC V5A 1S6, Canada
[2]Department of Chemistry, University of Victoria, Victoria, BC V8W 3V6, Canada
*Correspondence: plettner@sfu.ca
DOI 10.1016/j.chembiol.2009.01.005

SUMMARY

The pheromone-binding proteins (PBPs), which exist at a high concentration in the sensillum lymph surrounding olfactory neurons, are proposed to be important in pheromone detection and discrimination in insects. Here, we present a systematic study of PBP-ligand interaction kinetics. We find that PBP2, from the gypsy moth, *Lymantria dispar*, associates and dissociates slowly with its biofunctional ligands, (+)- and (−)-disparlure. Tryptophan anisotropy measurements detect PBP multimers in solution as well as an increase in the multimeric state of the protein upon long exposure to ligand. We propose a kinetic model that includes monomer/multimer equilibria and a two-step binding process: (1) external binding of the pheromone assisted by the C terminus of PBP2, and (2) slow embedding of the pheromone into the internal pocket. This experimentally derived model sheds light on the potential biological function and mechanism of PBPs as ligand scavengers.

INTRODUCTION

Communication with species-specific signal chemicals (pheromones) plays an important role in insect reproduction. For example, in the case of moths, the female releases the pheromone, and the males detect and follow the pheromone plume upwind to mate. The feather-like antennae of the moth act as a very sensitive chemoreceptor. The antenna is covered with hollow sensory hairs that are innervated by the dendrites of sensory neurons (sensilla). The cuticular hair wall is penetrated by a system of pore tubules that are thought to act as a pathway for the signal molecules passing from the outside of the hair to the interior (Steinbrecht, 1997). The lumen of the hair is filled with a protein-rich solution, the sensillum lymph. The most abundant proteins in the lymph of pheromone-sensitive hairs are the pheromone-binding proteins (PBPs) (Vogt and Riddiford, 1981) (Figure 1).

PBPs are small (~15 kDa), hydrophilic proteins that are specialized members of the insect odorant-binding protein (OBP) family. These proteins have been recently classified into three structural classes: long, medium, and short, differing mainly in the length of their C-terminal segment (Pesenti et al., 2008). Insect OBPs can bind odorants with some selectivity (reviewed: [Honson et al., 2005]); PBPs bind pheromone components. OBPs (including PBPs) are essential for insect olfaction (Kim et al., 1998). For example, OBP76a (LUSH) in *Drosophila* is required for vaccenyl acetate (cVA, a pheromone) detection (Ha and Smith, 2006; Xu et al., 2005) and has been further proven recently to adopt a conformation that activates the odorant receptor itself (Laughlin et al., 2008).

Although it is clear now that OBPs can actively present ligands to the receptor, there are other possible functions for OBPs. First, they can transport hydrophobic odorants across the lymph to the receptors (Krieger and Breer, 1999) (Figure 1). Second, the OBPs have been shown to be necessary for both neuronal background activity and odor-evoked activity (Benton et al., 2007; Grosse-Wilde et al., 2007; Laughlin et al., 2008; Xu et al., 2005). Third, OBPs may act as scavengers, buffering high doses of odorant and thereby preventing the neurons from saturating (Honson et al., 2003). The presence of multiple PBPs (Graham and Davies, 2002; Krieger et al., 1991; NagnanLeMeillour et al., 1996; Vogt et al., 1989) indicates that these proteins may also take part in the olfactory coding or signal filtering. Odorant receptors show different activity profiles for a set of ligands in the presence of different PBPs (Grosse-Wilde et al., 2007). PBPs bind individual pheromone components with subtle differences in the binding affinities (Du and Prestwich, 1995; Honson et al., 2003; Plettner et al., 2000). Also, PBPs have flexible binding pockets that can host a wide variety of compounds, but not all of the bound ligands seem to trigger an expedient conformational change of the protein (Kowcun et al., 2001; Lartigue et al., 2003; Lautenschlager et al., 2007; Pesenti et al., 2008). The question that arises now is: are these differences in equilibrium binding affinity functionally meaningful? OBP-ligand interactions require > 30 min to establish equilibrium (Plettner et al., 2000), whereas a moth responds to the pheromonal stimulus in milliseconds; thus, the interactions between the olfactory components (OBPs, ligands, and odorant receptors, etc.) may not be under thermodynamic control. The purpose of this work is to provide a dynamic perspective of the PBP functions.

Here, we focus on a lepidopteran, the gypsy moth, *Lymantria dispar*. The female gypsy moths emit (+)-disparlure ((*7R*, *8S*)-7,8-epoxy-2-methyloctadecane) as the main sex attractant pheromone component (Adler et al., 1972; Bierl et al., 1970, 1972). The antipode, (−)-disparlure, is a behavioral antagonist of upwind flight in gypsy moth males (Vite et al., 1976). The male

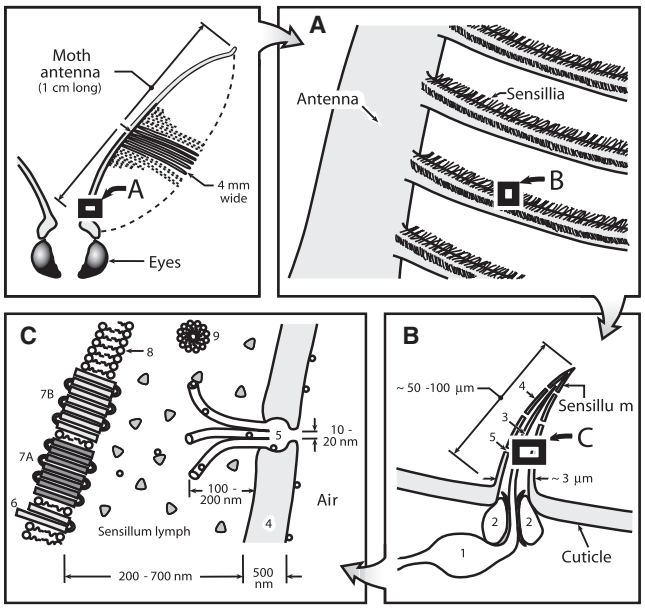

Figure 1. Schematic Illustrations of the Moth Olfactory System

(A) A close-up view of the hairy branches of moth antenna.

(B) Diagram of the olfactory sensillum ([1] olfactory receptor neuron; [2] auxillary supporting cells; [3] dendrite of an olfactory receptor neuron projecting into the hollow space of the sensillum; [4] cuticle wall of the hair; [5] cuticular pores).

(C) The peripheral components of the sensillum trichodeum ([6] sensory neuron membrane protein [SNMP]; [7] olfactory receptor and coreceptor; [8] phospholipid bilayer of the neuronal membrane; [9] micelles formed by fatty acids; shaded triangles, pheromone-binding proteins (PBPs); open circles, pheromone molecules). The pheromone molecules adsorbed on the cuticle wall of the sensillum migrate along the surface into the pore canal penetrating the cuticle and diffuse through the pore tubules into the sensillum lymph. PBPs come to interact with the ligands. The pheromone molecule may diffuse by itself through the barrier to associate with the membrane protein and then activate the receptor (Benton et al., 2007). Alternatively, ligand can either activate the PBP (Laughlin et al., 2008) or be delivered by the micelles (Honson, 2006).

moth antenna has separate sensilla populations specialized on either (+)-disparlure or on (−)-disparlure, but not both (Hansen, 1984). The gypsy moth has two known PBPs: LdisPBP1 and LdisPBP2 (PBP1 and PBP2 from here on). The sexual dimorphism, ontogeny (Vogt et al., 1989), and ligand binding affinities of these PBPs (Honson et al., 2003; Inkster et al., 2005; Kowcun et al., 2001; Paduraru et al., 2008; Plettner et al., 2000) have been studied. PBP2 binds (+)-disparlure slightly more strongly than (−)-disparlure. The timescale of PBP-ligand equilibration is much slower than the timescale at which individual insect sensilla are activated after the onset of a stimulus. Thus, kinetic studies are necessary to understand the mechanism of ligand binding and the biological function of PBPs.

In this paper, we report the first, to our knowledge, systematic study of the kinetics and mechanism for association and dissociation of physiologically significant pheromone compounds with PBP2. Our experimental approach relies on two techniques. First, we have applied our previous binding assay, in which bound and free ligand are separated by passage of the equilibrated mixture through a size-exclusion filter (Paduraru et al., 2008; Plettner et al., 2000). Second, we have developed a fluorescence assay, which relies on surface dansylation of the PBP and a decrease in dansyl (DNS) fluorescence upon ligand addition. Furthermore, since previous studies have suggested that PBPs multimerize (Danty et al., 1999; Honson et al., 2003; Leal, 2000; Maida et al., 1993; Plettner et al., 2000), we have also used Trp fluorescence anisotropy to examine the possible connection between PBP aggregation and ligand binding.

Our results indicate a two-step interaction process between PBP2 and ligand. A fast uptake of the hydrophobic ligand from the buffer is followed by slow embedding of the ligand into the binding pocket. The first process, rapid capture of the ligand on a millisecond timescale, has also been detected in a previous study with the PBP from the silk moth (*Bombyx mori*), BmorPBP (Leal et al., 2005). We have detected this rapid process indirectly (see below), and we have found no selectivity between (+)- and (−)-disparlure for PBP2. The second slow-binding step was found to be selective. Therefore, we have followed the second process, in which PBP2 shows similar discrimination between (+)- and (−)-disparlure in the kinetic constants (this paper) as in the dissociation constants (Plettner et al., 2000). We propose that the rapid-binding step mainly involves the C-terminal region of the protein, and that the slow-binding step mainly involves the core of the protein. This proposal is supported by the kinetics of a truncated form of PBP2 (T-PBP2) that lacks the 17 residues from the C terminus. Without the C-terminal peptide, T-PBP2 binds (+)-disparlure 10× weaker externally and exhibits much slower kinetic behavior. We believe that the C termini of long-chain PBPs play an important role in interactions with ligands. An effective conformational change could be triggered by a ligand either in the first step or the second step. In our simulation with all of the available kinetic constants, the results support that PBP does not need to associate quickly to produce sufficient PBP-ligand complex, i.e., properly shaped PBP (either $P.L_{ex}$ or P.L) (Equation 4), to activate the olfactory receptor (see Supplemental Data available online). We also present evidence for more than one population of PBP2 in solution. These populations are in equilibrium with each other and consist of high-order multimers. We propose a role for these multimers in ligand scavenging.

RESULTS

Ligand Binding Affinities of the Dansylated PBP2 and of the C Terminus-Truncated PBP2

The average amount of disparlure bound to dansylated PBP2 (DNS-PBP2) was compared to that bound to unlabeled PBP2. The result showed no statistically significant difference (six replicates, t test, $p > 0.05$, see Supplemental Data), and showed that the two proteins have very similar dissociation constants (Table 1). Therefore, the DNS modification did not affect the binding affinities of PBP2. This might be explained by the modification sites K31 and 38 being on the surface of the homology-modeled PBP2 structure. However, the C-terminally truncated PBP2, T-PBP2, exhibited a significantly reduced thermodynamic binding affinity toward (+)-disparlure (Table 1). Two observations suggest similar secondary structures for PBP2 and T-PBP2: (1) T-PBP2 reacts with antiserum raised against PBP2; and (2) both proteins have similar far-UV CD spectra (Figure S5). (Details of T-PBP2 preparation and conditions under which the K_Ds were measured can be found in Supplemental Data.)

Table 1. The Comparison of the Dissociation Constants between PBP2, DNS-PBP2, and T-PBP2 with (+)-Disparlure by GC Assay

Protein	$[P]_{total}$ (μM)	$[L]_{total}$ (μM)	$[L]_{bound}$ (μM)	$K_D = [L]_{free}[P]_{free}/[L]_{bound}$ (μM)
PBP2	2	4.7 ± 0.3	1.1 ± 0.2	2.9 ± 0.9
DNS-PBP2	2	3.8 ± 0.6	1.5 ± 0.5	2.6 ± 1.8
T-PBP2	2	0.6 ± 0.1	0.07 ± 0.01	16 ± 3

Means ± SE of six replicates.

Optical Properties of DNS-PBP2

When excited at 295 nm, DNS-PBP2 gives two emission peaks, assigned to Trp at 327 nm and DNS at 520 nm. The intensity of each is designated as I_{trp} and I_{dns} respectively (Figure 2A). The I_{dns}/I_{trp} ratio decreased significantly (>20%) upon ligand binding, dominated by a decrease in I_{dns}. With increasing concentration of ligand-bound protein, both I_{dns} and I_{trp} are observed to decrease linearly, although the change in I_{trp} is substantially smaller (Figure 2A). For this reason, subsequent experiments were conducted with selective excitation of DNS at 340 nm. The correlation between the change in I_{dns} and the concentration of ligand-bound protein is not dependent on total protein concentration; I_{dns} is observed to decrease with the same slope for either 2 or 4 μM protein (Figure 2B, procedures are described in Supplemental Data). Similar results were obtained with (+)-disparlure, (−)-disparlure, or the racemic mixture (data not shown). Since I_{dns} is more sensitive than I_{trp} to ligand binding, we have used I_{dns} to monitor the kinetics of protein-ligand association and dissociation.

Kinetic Studies

Association of DNS-PBP2 with (+)- and (−)-Disparlure

We have observed a slow association of ligands to PBP2 and DNS-PBP2, in seconds, and an even slower association to T-PBP2, in minutes (Figures 2C–2E). We consistently observed in both fluorescence and gas chromatography (GC) assays a non-zero physical quantity at time 0, which suggested some kinetic behavior of the protein that was not resolved on our experimental timescale (~5 s). This is clearly visible in our fluorescence assay (Figure 2C), in which ~50% of the total

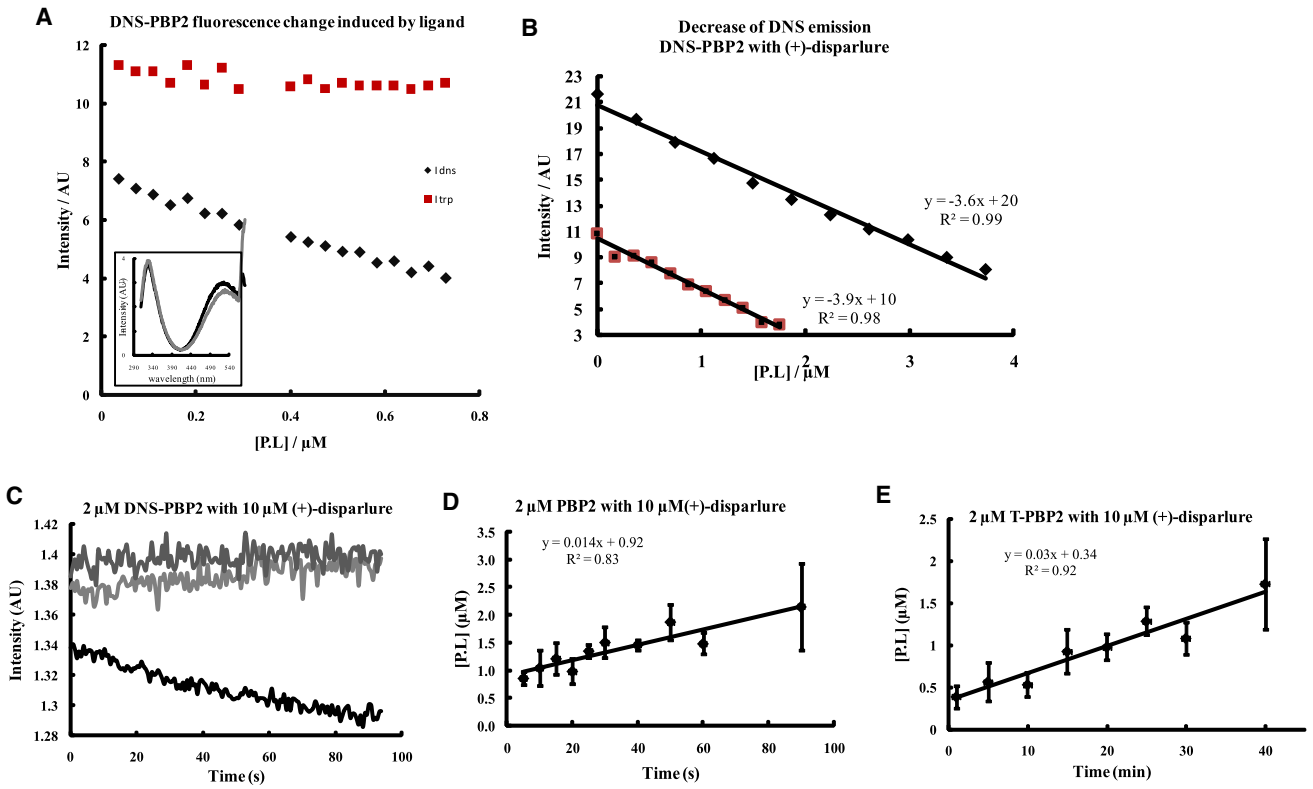

Figure 2. The Optical Properties of DNS-PBP2 Related to Ligand Binding and the Slow Association Kinetics of PBP2, DNS-PBP2, and T-PBP2

(A) An example to show the I_{trp} and I_{dns} change in tryptophan and dansyl fluorescence intensity, with increasing concentration of the protein-ligand complex for DNS-PBP2-(+)-disparlure, when the total protein concentration was kept at 2 μM. Samples were excited at 295 nm. The inset shows the spectra (black, without ligand; pale, with ligand).

(B) I_{dns} decreased linearly, corresponding to the increase in the concentration of ligand-bound protein. Samples were excited at 340 nm, for two different total protein concentrations (squares, 2 μM; diamonds, 4 μM).

(C) I_{dns} decreased with time upon ligand addition (black line), whereas the solvent for the ligand, EtOH, showed no effect (pale line, lower). The DNS fluorescence was stable with time when there was no treatment (pale line, upper).

(D and E) The association of (D) 2 μM PBP2 and (E) T-PBP2 with 10 μM (+)-disparlure determined by a GC assay (see Experimental Procedures). Each point represents the average of at least three replicates, and bars indicate the SE. The slope represents V_0, the initial binding velocity used in the determination of the order in Figure 3B. T-PBP2 shows much slower kinetics.

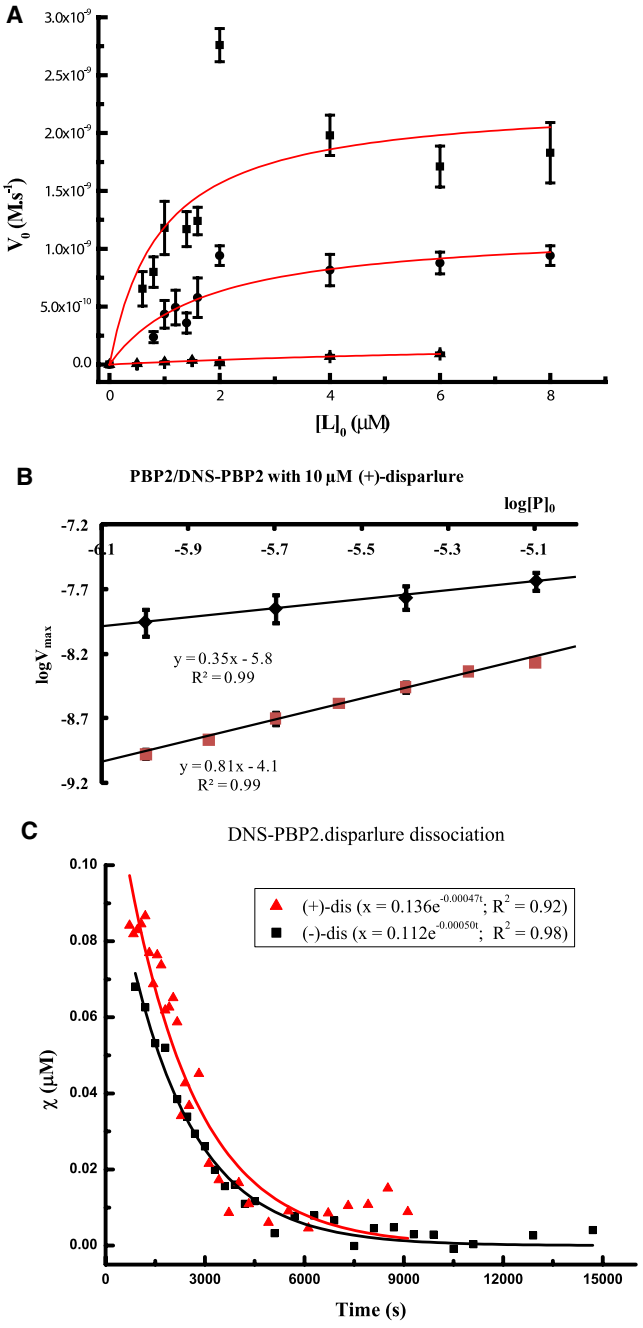

Figure 3. Binding Rates of PBP2 with (+)- or (−)-Disparlure and the Dissociation of DNS-PBP2-Ligand Complexes with Time

(A–C) For DNS-PBP2, rates were obtained by excitation at 340 nm and after changes in DNS fluorescence upon addition of ligand. For PBP2 and T-PBP2, rates were obtained from plots of GC-based data, such as the one in Figures 2D and 2E. Bars indicate SE for fluorescence-based data and fitting errors for GC-based data. (A) The plot of V_0 against L_0 when the protein concentration was 2 μM and the ligand concentration was varied between 0.6 and 8 μM. V_{max} is the maximal rate of ligand binding at ligand saturation. Curves are fitted to the Michaelis-Menten equation (squares, DNS-PBP2 and (+)-disparlure; circles, DNS-PBP2 and (−)-disparlure; triangles, T-PBP2 and (+)-disparlure). (B) Based on Equation 2, the plot of $\log V_{max}$ against $\log P_0$ when the ligand concentration was held constant at 10 μM and protein concentration was varied between 1 and 8 μM (diamonds, PBP2; squares, DNS-PBP2). The slopes give the reaction orders in protein, which are both smaller than 1 (see text). (C) The amount of the complex that is needed to be consumed to reach the final equilibrium was plotted against time (Equation 1). Fitting of the data to the first-order exponential decay presented the apparent dissociation rate constants, which are 4.7×10^{-4} s^{-1} for (+)-disparlure and 5.0×10^{-4} s^{-1} for (−)-disparlure. Fitting results are listed on the top right corner.

fluorescence quenching associated with ligand binding is static. Similar behavior is detected in our GC-based assay. The shortest feasible incubation time for GC-based assays is similar to the time resolution of the fluorescence experiments. Within this time window, we also observed by GC that ~40% of the total concentration of PBP2-ligand complexes (monitored over 100 s) had already formed (Figure 2D and Figure S6). We are unable to resolve the kinetics of PBP2 with (+)-disparlure in < 5 s with the current methods. However, we have carefully validated our measurements with different methods for the slower (>5 s) kinetic behavior, and the results are consistent.

In this work, we have probed the slow association by measuring the initial binding rate as a function of ligand concentration according to Equation 1:

$$V_0 = k_{on}[P]_0^m[L]_0^n, \quad (1)$$

where V_0 is the initial linear rate of the slow phase, k_{on} is the association constant, P_0 is the initial protein concentration, L_0 is the initial ligand concentration, and m and n reflect the reaction order of the protein and ligand, respectively. With increasing ligand concentration in the low-concentration regime in which ligand is limiting ($[L] \leq 2$ μM, 2 μM DNS-PBP2), the initial rate increased linearly. From the slope, we have obtained the k_{on} values for both ligands (Figure 3A). The reaction order, n for ligand, was obtained from the slope of a plot of $\log V_0$ versus $\log[L]_0$ (Table 2). At ligand concentrations exceeding that of protein, V_0 becomes independent of ligand concentration. This result is very important. It indicates that PBP2 becomes saturated with excess ligand and reaches its maximum association velocity, which is independent of the ligand concentration. We have observed an offline point at 2 μM ligand for both ligands, in both methods. This is consistent with our previous observation that binding affinity is related to the protein:ligand ratio (Honson et al., 2003). One explanation is that PBP acts differently at high and low ligand concentration, and that 2 μM, corresponding to 1:1 PBP:ligand ratio in our case, is a switch point for different PBP functions.

In a second series of experiments, the protein concentration was varied from 1 to 8 μM, whereas the ligand concentration was in constant excess (10 μM). The initial rates thus obtained correspond to the maximum at each protein concentration. These are shown in Figure 3B derived from fluorescence and GC assays. These data may be fit to Equation 2:

$$\log V_{max} = \log k + m \log P_0, \quad (2)$$

where m represents the general "association" order of the protein, whereas the parameter k typically represents the rate constant. The meaning of this parameter for PBP2 ligand binding will be discussed below. The association orders for PBP2 from either fluorescence (0.81 ± 0.03) or GC (0.35 ± 0.02) assays are both smaller than 1 (Table 2).

Table 2. Summary of Ligand-Binding Kinetics and Thermodynamics for PBP2

Measurement		Ligand	
		(+)-Disparlure	(−)-Disparlure
k_{on} /$M^{-1}s^{-1}$[a]	DNS-PBP2	$(4.8 \pm 0.4) \times 10^2$	$(1.6 \pm 0.2) \times 10^2$
	T-PBP2	$(0.12 \pm 0.01) \times 10^2$	N.D.[b]
k_{off} /s^{-1}[a]	Flu.	$(4.7 \pm 0.4) \times 10^{-4}$	$(5.0 \pm 0.2) \times 10^{-4}$
	Radio[c]	1×10^{-4}	3.3×10^{-5}
n		1.1 ± 0.2	1.3 ± 0.3
K_D/μM	Flu. k_{off}/k_{on}	1.0	3.1
	Radio[c]	1.8	3.2
K_D'/μM[d]	DNS-PBP2	0.9 ± 0.5	1.6 ± 0.6
	T-PBP2	10 ± 3	N.D.
k_2/s^{-1}[e]	DNS-PBP2	4.3×10^{-4}	2.6×10^{-4}
	T-PBP2	1.5×10^{-4}	N.D.
m	Flu.	0.81 ± 0.03	N.D.
	GC	0.35 ± 0.02	N.D.

[a] $V_{on} = k_{on}[P]^m[L]^n$; $V_{off} = k_{off}[P \cdot L]$.
[b] N.D., not determined.
[c] Assays with radio-labeled disparlure (Honson et al., 2005; Plettner et al., 2000).
[d] The dissociation constant of the hypothetical intermediate $P \cdot L_{ex}$ from the fitting of PBP2 association data (Figure 3A) with the Michaelis-Menten equation:

$$K_M = \frac{k_{-1} + k_2}{k_1} \approx \frac{k_{-1}}{k_2} = k_D'.$$

[e] $k_2 = K_D' \times k_{on}$ (Equation 4).

The association curve of T-PBP2 with (+)-disparlure is very similar to that of PBP2 (Figures 2E and 3A), except that the binding is much slower (for experimental procedures, see Supplemental Data).

Dissociation of DNS-PBP2-Ligand Complexes

Dissociation of DNS-PBP2-ligand complexes (Figure 3C) follows an apparent first-order exponential decay (Equation 3, derived in Supplemental Data):

$$x = Ae^{-k_{app}t}, \quad (3)$$

where x represents the amount of complex dissociated to reach the final equilibrium, and k_{app} is the apparent dissociation rate constant, k_{off}. DNS-PBP2 complexes with either (+)- or (−)-disparlure dissociate with similar, extremely slow, kinetics (Table 2). Our rate constants for ligand binding and release yield dissociation constants ($K_D = k_{off}/k_{on}$, Table 2) that compare well to literature values of 1.8 and 3.2 μM for (+)- and (−)-disparlure, respectively (Plettner et al., 2000). The slight selectivity between these two ligands was preserved. That is, PBP2 binds (+)-disparlure more strongly than (−)-disparlure, either in equilibrated conditions or as indicated from the derived kinetic constants. These results are important, as they indicate that the processes we are following represent the rate-limiting steps for binding and dissociation.

Molecular Size of PBP2-Ligand Complexes Evaluated by Tryptophan Anisotropy

We have measured the Trp fluorescence anisotropy of unlabeled PBP2, and its ligand complexes, as a function of solvent viscosity in order to evaluate their hydrodynamic volumes and, correspondingly, their degree of multimerization. Double reciprocal plots of anisotropy versus viscosity are linear, as predicted by Equation S6 (Figure S8). To extract the volume, V, from these data, we also require the limiting anisotropy, r_0, and fluorescence lifetime, τ, of Trp in each sample and the hydrodynamic volume of monomeric PBP. The former, r_0, was obtained from the linear fitting of the data, and τ (Table 3) has been measured experimentally (Supplemental Data). The hydrodynamic volume of monomeric PBP2 is estimated to be 29 nm^3 according to Equation S7. Based on crystallographic data, the approximate dimensions of the PBP from the silkworm moth *Bombyx mori* (BmorPBP) (15.9 kDa, 142 aa) are 40 × 35 × 30 Å (Sandler et al., 2000). Its corresponding volume, approximating an ellipsoid, is 22.0 nm^3. Considering that PBP2 (16 kDa, 145 aa) is longer by 3 amino acids than BmorPBP, the calculated 29 nm^3 volume for PBP2 monomer is reasonable.

Hydrodynamic volumes of PBP2 and its complexes are evaluated according to Equation S6, yielding values ranging between ~40 and 90 nm^3 depending on protein concentration and ligand incubation time (Table 3). Within experimental error (±5 nm^3), the average hydrodynamic volume of apo-PBP2 was independent of protein concentration between 2 and 10 μM, and the averaged volume for an overall population of PBP2 (free and ligand-bound forms) was unchanged by short incubation with ligand. A consistent increase in volume was detected after overnight incubation with ligand.

In all cases, the numbers of monomers in each rotational unit (evaluated as $V_{sample}/V_{monomer}$) are nonintegral. This is not surprising given that we are measuring the average molecular volume of an equilibrium population of PBP2 species, e.g.,

Table 3. Trp Anisotropy Parameters for PBP2 and PBP2-(+)-Disparlure Complexes after Different Incubation Conditions

Conditions	2 μM			10 μM		
	Without Ligand	3 min Incubation	Overnight	Without Ligand	3 min Incubation	Overnight
r_0	0.08	0.07	0.07	0.04	0.05	0.07
τ/ns[a]	4.95	4.39[b]	3.82	4.83	4.79[b]	4.74
V/nm^3	52.6	54.7	67.1	44.9	43.0	87.5
Number of monomers[c]	1.8 ± 0.1	1.9 ± 0.01	2.3 ± 0.2	1.5 ± 0.3	1.5 ± 0.2	3.0 ± 0.8

[a] Amplitude average lifetime.
[b] Average of the lifetimes obtained without ligand and incubated with ligand overnight.
[c] $V_{sample}/V_{monomer}$.

monomer and dimer. We further note the errors associated with these measurements and the theoretical approximations made, including modeling the rotating particle as a sphere. However, in all cases, the number of monomers is greater than unity, largely between 1 and 2 within experimental error. This consistently suggests that PBP2 does not exist as homogenous monomers in solution, either with or without ligand; instead, an equilibrium population of monomers and dimers is the simplest explanation for our data. The change of the multimerization equilibrium induced by ligand was significantly slower than the binding kinetics. Therefore, the change in multimer states during the time window of the binding kinetics was insignificant, simplifying data analysis.

DISCUSSION

Fluorescent PBP2 Mimics Wild-Type Protein

As confirmed by the GC assay, PBP2 and DNS-PBP2 have the same dissociation constants within experimental error (Table 1); the modification does not change the binding affinities of PBP2. It is therefore likely that the binding pocket and corresponding ligand interactions are unaffected by the fluorophore, consistent with the labeling sites (K31 and/or K38) being on the surface of the protein. Furthermore, two different methods, GC and fluorescence, gave fractional association orders, m, for PBP2 with (+)-disparlure (Figure 3B), and K_D values estimated from k_{on} and k_{off} for both ligands are close to those previously reported (Table 2). Thus, the fluorescent-labeled PBP2 is a valid mimic of wild-type protein and provides a method for measurements of native ligand binding kinetics.

Kinetic Pathway for the PBP2-Ligand Interaction

Previous studies have found that a decrease of the pH can induce a significant conformational change on the C termini of long-chain PBPs (Damberger et al., 2007). The newly formed seventh α helix then occupies the binding pocket and therefore is proposed to be responsible for the release of the ligand near the olfactory neuron membrane, where the pH is assumed to be significantly lower than the lymph pH. However, from a more recent study, it seems that a small local conformational change of the PBP (not caused by pH changes) is sufficient to trigger the receptor response (Laughlin et al., 2008). We did not investigate the pH effect on PBP-ligand interaction kinetics in this paper. Based on the behaviors of PBP2 under physiological pH we have found here, we propose an alternative pathway of ligand binding and releasing, without invoking a significant conformational change of the C terminus induced by a pH decrease.

Based on the measured association and dissociation kinetics of DNS-PBP2 with (+)- and (−)-disparlure, we propose that PBP2 associates with the ligand first at a peripheral site, building equilibrium promptly with the rate constants k_1 and k_{-1} for the forward and reverse interactions, respectively (Equation 4). The PBP2-ligand complex intermediate, $P{\cdot}L_{ex}$, may then be transformed to the specific complex $P{\cdot}L$, by properly orienting the ligand and docking it into the inner binding pocket. The rate constant for this step is designated as k_2. Complex $P{\cdot}L$ dissociates to the intermediate $P{\cdot}L_{ex}$ with a very small rate constant, k_{-2} (Equation 4). The rate-limiting step for binding is internalization of the initially associated ligand, whereas exhalation of the bound ligand to the peripherally associated species rate limits the dissociation process ($k_1 \gg k_2$, $k_{-1} \gg k_{-2}$):

$$P + L \underset{k_{-1}}{\overset{k_1}{\rightleftarrows}} P{\cdot}L_{ex} \underset{k_{-2}}{\overset{k_2}{\rightleftarrows}} P{\cdot}L. \quad (4)$$

The proposed intermediate in the binding pathway is necessary to rationalize the saturability of the association curves observed in both fluorescence and GC-based assays (Figure 3A). Two-phase binding kinetics have been observed during earlier work on PBPs (Honson et al., 2005; Leal et al., 2005), and a similar ligand-binding pathway has been observed for human cytochrome P450 3A4 (Isin and Guengerich, 2007), for which substrate binds to a peripheral site before entering the catalytic pocket. Here, we find that the initial association proceeds at a fast rate, which cannot be resolved on the timescale we are using, suggesting that it is more easily accessed by ligand. Our recent results with a fluorescent ligand and stopped-flow measurements confirm the existence of this fast step (unpublished data). We propose that this first binding site is a hydrophobic patch on the protein surface, specifically a site near the C terminus of the PBP. This model is based on several facts. First, the C terminus is sufficiently hydrophobic to accommodate the aliphatic chain of the ligand (Figure 4A). Second, the flexibility of the C terminus provides a greater opportunity for protein-ligand collision than the less flexible core of the protein. Third, the C terminus, the N terminus, and the loop between α helices 2 and 3 comprise an opening of the binding pocket with considerable mobility (Zubkov et al., 2005). Our proposed model is also supported by two other pieces of experimental data. First, in the photoaffinity labeling of *Antheraea polyphemus* PBP (ApolPBP) with an analog of its pheromone, the exclusively labeled residue (Thr44) is located on the α2/α3 loop in a conformation pointing outward relative to the binding pocket (Du and Prestwich, 1995; Mohanty et al., 2004). Second and most importantly, the ~40× slower kinetic behavior of T-PBP2 (this study) indicates damage to the association phase when the C terminus is missing (Table 2).

We also suggest that the external binding site possibly involves Trp37, which is highly conserved in all long-chain PBPs and is in the α2-α3 loop (Figures 4A and 4B). Assays of ligand binding based on changes in Trp fluorescence are consistent with our proposed two-step binding model. Binding of bombykol, the cognate ligand for BmorPBP, was shown to quench the intrinsic Trp fluorescence of BmorPBP in milliseconds with no spectral shift (Leal et al., 2005). Also, titration of ligand into ApolPBP elicited a change of the Trp37 fluorescence intensity with no shift in emission wavelength (Bette et al., 2002). These changes in Trp fluorescence intensity with no spectral shift appear to be characteristic of a rapid interaction between a ligand and the external binding site.

The process of ligand translocation from the external, peripheral site to the internal binding pocket has been the focus of the current kinetic study. Due to technical problems with adsorption of very hydrophobic ligands in the stopped-flow fluorimeter, we have put our efforts toward studying the slow step. We have observed the first step, using a more soluble fluorescent dye as a surrogate ligand (unpublished data). With DNS-PBP2 and disparlure, we could not separate the initial association from

A

```
ApolPBP          SPEIMKNLSNNFGKAMDQCKDELSLPDSVVADLYNFWKDDYVMTDRLAGCAINCLATKLD 60
AperPBP          SPEIIKNLSQNFCKAMDQCKQELNIPDSVIADLYNFWKDDYVMTDRLAGCAINCMATKLD 60
BmorPBP          SQEVMKNLSLNFGKALDECKKEMTLTDAINEDFYNFWKEGYEIKNRETGCAIMCLSTKLN 60
AvelPBP          SQDVIKGMTLNFRKGLDECKKEMNLPDSINADFYNFWKDDHVLSNRDTGCAIMCLSSKLE 60
HvirPBP          SQDVMKNLSMNFAKPLEDCKKEMDLPDSVTTDFYNFWKEGYEFTNRHTGCAILCLSSKLE 60
LdisPBP1         SKEVMKQMTINFAKPMEACKQELNVPDAVMQDFFNFWKEGYQITNREAGCVILCLAKKLE 60
LdisPBP2         SKDVMHQMALKFGKPIKLCQQELGADDSVVKEFLDFWKDGYVMKDRQTGCMLICMAMKLE 60
                 * :::: :: :* * :. *:.*:   *::  :: :***:.: :.:* :** : *:: **:

ApolPBP          VVDPDGNLHHGNAKDFAMKHGADETMAQQLVDIIHGCEKSAPPN--DDKCMKTIDVAMCF 118
AperPBP          VVDPDGNLHHGNAKEFAMKHGADASMAQQLVDIIHGCEKSAPPN--DDKCMKTIDVAMCF 118
BmorPBP          MLDPEGNLHHGNAMEFAKKHGADETMAQQLIDIVHGCEKSTPAN--DDKCIWTLGVATCF 118
AvelPBP          LVS-DGKLHHGNTFDYAKQHGADETVAQQLVDLIHSCEKSLPDL--EDPCMKVLEWAKCF 117
HvirPBP          LLDQEMKLHHGKAQEFAKKHGADDAMAKQLVDMIHGCSQSTPDAT-DDPCMKALNVAKCF 119
LdisPBP1         LLDQDMNLHHGKAMEFAMKHGADEAMAKQLLDIKHSCEKVITIVA-DDPCQTMLNLAMCF 119
LdisPBP2         LLDSAMEIHHGSTFAFAKAHGADEAMAQQIIDIVHGCTTTYPAAETNDPCQRAVNVAMCF 120
                 ::.   ::***.:  :*  **** ::*:*::*: *.*    .    :* *   :  * **

ApolPBP          KKEIHKLNWVPNMDLVIGEVLAEV- 142
AperPBP          KKEIHKLNWVPDMDVVLGEVLAEV- 142
BmorPBP          KAEIHKLNWAPSMDVAVGEILAEV- 142
AvelPBP          KTEIHKLNWAPSVEVLAAEMLAEV- 141
HvirPBP          KAKIHELNWAPSMELVVGEVLAEV- 143
LdisPBP1         KAEIHKLDWAPTLDVAVGELLADT- 143
LdisPBP2         KAHVHKLNWAPDVELLVADFLAESQ 145
                 * .:*:*:*.* :::  .:.**:
```

B

C

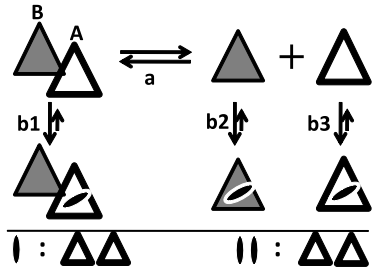

Figure 4. Sequence Alignments and Models

(A) Sequence alignments of the PBPs of the moths *Antheraea polyphemus*, *A. pernyi*, *Argyrotaenia velutinana*, *Bombyx mori*, *Heliothis virescens*, and *Lymantria dispar*. An asterisk indicates a fully conserved residue, a colon specifies strongly conserved residues, and a period indicates a weakly conserved residue. Overall, the C termini of the long-chain PBPs, starting from the second framed Trp, share high similarity and are considerably hydrophobic.

(B) The threading structures of PBP2 on 20 of the NMR structures of BmorPBP (PDB ID: 1LS8) (left) (Lee et al., 2002) and ApolPBP (PDB ID: 1QWV) (right) (Mohanty et al., 2004). Trp37 and Trp129 are shown. The C terminus and the loop between α helices 2 and 3 present multiple conformations. Models were prepared with Spdb-viewer.

(C) Model of the equilibrium between the PBP dimer and monomer. Addition of ligand or high protein concentration favors the formation of dimers (step a), in which two populations of PBP exist (type A and type B). Type B PBP has a more blocked ligand entrance to the inner binding site. The binding process of PBP molecules is labeled as step b. Dimeric PBP has smaller binding capacity (one ligand per two proteins) than the monomeric PBP (one ligand per protein) (ellipses, ligand; triangles, PBP). The binding capacity is shown schematically below the line.

the translocation process. However, the overall binding process is saturable (Figure 3A), meaning that a steady-state population of the intermediate ($P \cdot L_{ex}$) builds up rapidly, and that the externally adsorbed ligand is then slowly internalized. The k_{on} values obtained represent the overall rate constant for both steps. The overall process (Equation 4) is analogous to a pathway for one-site enzyme catalysis. A plot of the initial rate against ligand concentration at constant protein concentration may thus be fit to the Michealis-Menten equation to estimate the K_M value. This will be close to the dissociation constant, K'_D, of the intermediate when $k_{-1} \gg k_2$ (Table 2). This is related to the concentration of the intermediate, Equation 5,

$$[P \cdot L_{ex}] = \frac{[P][L]}{K'_D} \approx \frac{[P][L]}{K_M}, \quad (5)$$

and, correspondingly, to the overall rate constant for ligand binding, k_{on}, Equation 6,

$$V_{on} = \frac{d[P \cdot L]}{dt} = k_2[P \cdot L_{ex}] \approx \frac{k_2}{K_M}[P][L] = k_{on}[P][L]. \quad (6)$$

The values of K'_d for (+)- and (−)-disparlure with DNS-PBP2 are similar, (0.9 ± 0.5) μM and (1.6 ± 0.6) μM, respectively. However, the binding affinity of (+)-disparlure at the peripheral site of T-PBP2 is 10× weaker (K'_D = 10 μM). This agrees well with the hypothesis that the C terminus is the major component of the peripheral binding site. The translocation rate constant k_2, as a product of K'_D and k_{on}, is a first-order rate constant with the unit of s^{-1}. The k_2 values show slight difference between ligands (4.3×10^{-4} s^{-1} for (+)-disparlure and 2.6×10^{-4} s^{-1} for (−)-disparlure), suggesting that the slow second translocation step is ligand selective. This value for T-PBP2 with (+)-disparlure is smaller (1.5×10^{-4} s^{-1}), which means that the loss of the C terminus affected the internalization of the ligand to some extent (Table 2).

The dissociation of the P·L complex is extremely slow. This is likely caused by complete enclosure of the ligand in the binding pocket, such as bombykol in BmorPBP and cVA in LUSH (Laughlin et al., 2008; Sandler et al., 2000). Furthermore, our observation that T-PBP2 dissociates from ligand more easily (larger K_D, Table 1) indicates that the removal of the C terminus has lowered the barrier to dissociation. Recent research has shown the importance of the subtle conformational changes of the C termini of medium-chain PBPs induced by ligand binding (Laughlin et al., 2008; Pesenti et al., 2008). This could also be the case for the C termini in the long-chain PBPs. Based on our study, we propose that the C terminus and the other components of the external binding site may act as a stepping stone that assists the entry of the ligand into the interior binding pocket, as well as a "gate" that may "lock" the ligand inside and make dissociation difficult.

Monomer and Multimer Equilibrium in Solution

Aggregation of OBPs in solution has been reported several times (Danty et al., 1999; Honson et al., 2003; Leal, 2000; Plettner et al., 2000) and has been observed directly in the solid state by X-ray crystallography (Kruse et al., 2003; Lartigue et al., 2003, 2004; Laughlin et al., 2008; Sandler et al., 2000). Since the oligomeric state of the proteins may affect the interactions with ligand, we need to understand the aggregation forms of the PBP under the kinetic test conditions. We propose that, in solution, the PBP monomer exists in equilibrium with at least one other population of higher-order aggregate, most likely a dimer under our experimental conditions. This proposal is supported by values for PBP2 hydrodynamic volumes, estimated by Trp fluorescence anisotropy, that are intermediate between monomeric and dimeric forms, even at a low concentration of 2 μM (Table 3).

Additional evidence for protein multimerization comes from measurements of the initial association rate of PBP2 with an excess of ligand, which provides the maximum rate, V_{max}, at that protein concentration (Figure 3B). We found that V_{max} is proportional to $[P]^m$, $m < 1$ (Table 2), which means that $V_{max}/[P]$ will decrease with increasing protein concentration. Since V_{max} represents the maximum number of ligand molecules that can be bound to the protein per second, $V_{max}/[P]$ represents the maximum number of bound ligand molecules per protein molecule per second—in other words, the binding capacity of the PBP per second. At increased protein concentration, this binding capacity decreases. One explanation is that, at high protein concentration, the aggregated protein blocks the binding of ligand to some extent. If there are two populations of protein in the solution (Figure 4C), they may or may not have the same conformation. One population of PBP can bind ligand directly (A in steps b1 and b3), whereas another, whose binding pocket is blocked in the multimeric form, needs to dissociate first (B in step b2). The monomer-multimer equilibrium will shift toward multimer with increasing protein concentration (step a), accounting for the decreased per-second binding capacity in the higher protein concentration regime.

Consequently, we suggest addition of another component to the core PBP2 kinetics scheme, namely, equilibrium between monomeric and dimer/multimeric forms of PBP2. The shift of this equilibrium induced by ligand is slow and therefore will not interfere with the PBP-ligand interaction kinetics. Steady-state kinetics do not resolve the equilibrium distribution; our measurements reflect the population-weighted average kinetic properties of all PBP2 species, of which only ligand-binding-competent type A are represented by P in Equation 4.

The maximal initial velocity measured by both fluorescence and GC methods (Figure 3B) corresponds to the $P_A \cdot L_{ex}$ concentration at its maximum. In excess ligand, the concentration of the intermediate $P_A \cdot L_{ex}$ is proportional to the concentration of P_A, which is linked to the initial protein concentration, P_0, and the dimer-monomer equilibrium constant. Since we have no information on the latter, we make no attempt to derive or solve an expression for the parameter k in Equation 2. Considering the high concentration of PBPs in the sensillum lymph (average of ~600 μM for LdisPBPs [Honson, 2006]), it is unlikely that PBP will reach maximum velocity at odorant doses encountered in typical plumes. These doses range from 10 molecules·s^{-1}·sensillum^{-1} (17 pM) to ~10^8 molecules·s^{-1}·sensillum^{-1} (170 μM) (Supplemental Data).

Multifunctional PBPs

Based on previous work, C terminally activated PBP can be an activator of pheromone-sensitive neurons (Laughlin et al., 2008). Our study reveals two-step association kinetics of a ligand with PBP2 and indicates a role of the C terminus in ligand

binding. The rapid phase is proposed to involve the uptake of the ligand by the C terminus of PBP2, whereas the slow phase is proposed to involve specific internalization of the ligand into the binding pocket. The selectivity of this slow step parallels the thermodynamic binding selectivity of PBP2 with different ligands, consistent with the observation that pheromone ligand can specifically trigger an active conformation of the PBP (Laughlin et al., 2008). However, the selectivity here is still not strong enough to count for the high specificity of the moth olfactory system. Therefore, as indicated by Laughlin et al. (2008) and Pesenti et al. (2008), the selectivity of the peripheral olfaction may rely on the differences of the C-terminal conformations of PBPs with different ligands. In our hypothesis, the insect olfactory sensing may not be under thermodynamic, but kinetic, control. The most active ligand might be the one that most efficiently triggers the C terminus conformational change. We do not know at which stage the C terminus of the PBP is activated—the external binding stage or the internal binding stage. However, because the odorant receptor is sensitive enough to detect a few molecules, sufficient amount of $P{\cdot}L_{ex}$ or $P{\cdot}L$ complexes could be formed in milliseconds, even for a slow-binding protein such as PBP2 (Figure S9). Another PBP from the same species, PBP1, binds ligand ~2× faster (unpublished data).

In addition to a ligand transporter and activator, PBP may also act as a scavenger. PBPs can multimerize into an asymmetric dimer. Each monomer of this asymmetrical unit presents a different conformation of the C terminus (Laughlin et al., 2008; Sandler et al., 2000). Specifically, it is the monomer B (whose C terminus is relatively more blocked) that retains the active conformation when a ligand is bound (Laughlin et al., 2008). The active conformation could very possibly be deactivated through PBP dimerization. We have observed slow multimerization of PBP2, and we hypothesize that, at high ligand concentration, this could be one mechanism used to protect the receptors from being saturated.

SIGNIFICANCE

Odorant-binding proteins play a significant role in odorant detection in insects. Pheromone-binding proteins, PBPs, are members of this protein family, specialized in binding pheromones. Various biological functions have been proposed for PBPs, and a lot of their static properties have been unveiled, such as the 3D structures and binding affinities with different ligands. However, little effort has been made to understand the dynamic interactions between a PBP and a ligand. To our knowledge, we have presented here the first systematic kinetic study on the interaction between one PBP, PBP2, from the gypsy moth, with its natural ligands, (+)- and (−)-disparlure.

We have shown that PBP2, which belongs to the "long" category PBPs (with ~12–15 aa hydrophobic C-terminal peptide), binds hydrophobic ligands in two steps: one rapid, the other slow. We suggest that the slow one corresponds to the specific reorienting and embedding of the ligand to the internal binding pocket, whereas the rapid one is from the binding to an external site close to the C terminus. Based on recent literature (Laughlin et al., 2008), the PBP-ligand complex, with ligand bound at an internal site, is an active ligand of the odorant receptor.

Our study has revealed an important role for the C terminus of long-chain PBPs: to act as a gate and as part of a path for the ligand. We also provide more evidence for the existence of PBP multimers in solution, and we provide new, to our knowledge, evidence that, over a long time (hours), the multimerization state increases in the presence of ligand. Our results support the hypothesis that, in addition to a carrier of ligand, PBP is also a scavenger.

EXPERIMENTAL PROCEDURES

Preparation of Dansylated PBP2

PBP2 was expressed and purified as previously described (Plettner et al., 2000) and was stored at −37°C in 20 mM Tris-HCl buffer (pH 7.4). Before the reaction, 10 ml of 30–50 μM PBP2 solution was dialyzed against 2 × 1 L 20 mM $NaHCO_3$ buffer (pH 10.3) overnight at 4°C, to replace the Tris. Two times excess of 53.0 mM fresh dansyl chloride (DNS-Cl) in EtOH was slowly added to the protein solution every half hour. The reaction was conducted at room temperature on a stirring plate and stopped after 1 hr by running the crude product on preparative 12% native PAGE gels directly. Fluorescent fractions were pooled together and dialyzed against 20 mM Tris-HCl buffer (pH 7.4). The dansylation was confirmed by MALDI mass spectrometry, the composition, with respect to the number of dansyl groups attached (see Supplemental Data), was evaluated by FPLC, and the attachment sites (K31 and 38) were identified by peptide mapping (Table S3). The apparent molecular weights of the protein samples were calculated according to their compositions. Extinction coefficients at 280 nm, ε_{280}, evaluated from known quantities of pure nondansylated and dansylated PBP2 compare well to calculated estimates, which are based on the amino acid composition of the PBP2 (Pace et al., 1995) and the absorbance of DNS group at 280 nm (ε_{280} = 1920 $M^{-1}cm^{-1}$ for dansyl t-butylamine):

$$\varepsilon(280)\left(M^{-1}cm^{-1}\right) = 5500 \times (\#Trp) + 1490 \times (\#Tyr) + 125 \times (\#Cys) + 1920 \times (\#DNS)$$

(#Trp = 2, #Tyr = 2, #Cys = 6, #DNS = $\sum_0^i a_i(\#DNS)_i$) (Table S3). The experimentally measured ε_{280} values were used to evaluate protein concentration. All protein samples used for the experiments were in 20 mM Tris-HCl buffer (pH 7.4) unless otherwise indicated.

Association of DNS-PBP2 with (+)- and (−)-Disparlure

Ligand association with DNS-PBP2 was investigated at a constant protein concentration (2 μM) with varied ligand concentrations (0.6–8 μM), and also at a constant ligand concentration (excess, 10 μM) with varied protein concentration (1–8 μM). Each protein sample was equilibrated in the fluorescence cuvette for at least 2 min before ligand addition, and all measurements were made at 20°C. At least four replicates were performed. Controls, in which the same volume of EtOH was added to the protein as that of the ligand stock, were performed in parallel. Samples were excited at 340 nm, and the emission of DNS-PBP2 was monitored at 522 nm one point per second for at least 90 s.

To validate the optical measurements, we have performed a second series of experiments, in which the protein concentration was varied and the ligand concentration was constant and in excess by using a GC assay. In this assay, 100 μl PBP2 samples of 1, 2, 4, and 8 μM were incubated with 10 μM (+)-disparlure (1 μl of 1 mM ethanol stock) for various lengths of time (5–90 s), and each point was tested in triplicate. Pheromone bound to PBP was separated from the free pheromone by gel filtration on small columns of Bio-Gel P2 (0.06 g) in a 200 μl pipette tip. The filtrate was extracted with 2× 50 μl hexane:ethyl acetate (1:1) mixture, and the recovered ligand was quantitated by GC.

Dissociation of DNS-PBP2 with (+)- and (−)-Disparlure

The DNS-PBP-ligand complexes were obtained after an overnight incubation as described above, and they were diluted to the desired concentration of 2 μM. The DNS fluorescence intensity was monitored immediately after preparation for about 3 hr at 20°C. Dissociation rate constants were obtained by fitting the data to an exponential decay.

Tryptophan Anisotropy Measurements

Samples (20 mM Tris buffer [pH 7.4]) were prepared as described by Flecha and Levi (2003), and sample viscosity was varied with glycerol, by using the same composition for each set of samples (four replicates). Two protein concentrations (2 and 10 μM) were chosen. Experiments were conducted without ligand and with 10 μM of the most strongly bound ligand for each protein. Ligand-containing samples were measured after 3 min and again after overnight incubation. Tryptophan was excited at 280 nm, and its emission was monitored at 335 nm (20°C) by using a HORIBA Jobin Yvon SPEX spectrofluorometer (Fluorolog-3) equipped with Glan-Thompson autopolarizers (5 nm bandwidth). Reported anisotropy values, determined from the intensity of the horizontally (H) and vertically (V) polarized emission components according to Equation 7, are averages of at least three measurements:

$$r = \frac{I_{VV} - G \cdot I_{VH}}{I_{VV} + 2 \cdot G \cdot I_{VH}}, \text{ with } G = \frac{I_{HV}}{I_{HH}}. \quad (7)$$

SUPPLEMENTAL DATA

Supplemental Data include Supplemental Experimental Procedures, Supplemental References, nine figures, and three tables and are available with this article online at http://www.cell.com/chemistry-biology/supplemental/S1074-5521(09)00029-5.

ACKNOWLEDGMENTS

We thank J. Huang for the help with peptide mapping and Q. Yang (School of Engineering Science, Simon Fraser University, Burnaby, British Columbia) for the help with mathematics in Equation 3. This work was supported by the Natural Sciences and Engineering Research Council of Canada (NSERC) for C.B., a Canada Graduate Scholarship for NSERC for T.C.S.P., and RGPIN222923 (NSERC Operating) and STGRP307515 (NSERC Strategic) for E.P.

Received: October 31, 2008
Revised: December 25, 2008
Accepted: January 13, 2009
Published: February 26, 2009

REFERENCES

Adler, V.E., Bierl, B.A., Beroza, M., and Sarmient, R. (1972). Electroantennograms and field attraction of gypsy moth Lepidoptera-Lymantriidae sex attractant disparlure and related compounds. J. Econ. Entomol. *65*, 679–680.

Benton, R., Vannice, K.S., and Vosshall, L.B. (2007). An essential role for a CD36-related receptor in pheromone detection in *Drosophila*. Nature *450*, 289–293.

Bette, S., Breer, H., and Krieger, J. (2002). Probing a pheromone binding protein of the silkmoth *Antheraea polyphemus* by endogenous tryptophan fluorescence. Insect Biochem. Mol. Biol. *32*, 241–246.

Bierl, B.A., Beroza, M., and Collier, C.W. (1970). Potent sex attractant of gypsy moth: its isolation, identification, and synthesis. Science *170*, 87–89.

Bierl, B.A., Beroza, M., and Collier, C.W. (1972). Isolation, identification, and synthesis of gypsy moth Lepidoptera-Lymantriidae sex attractant. J. Econ. Entomol. *65*, 659.

Damberger, F.F., Ishida, Y., Leal, W.S., and Wuethrich, K. (2007). Structural basis of ligand binding and release in insect pheromone-binding proteins: NMR structure of *Antheraea polyphemus* PBP1 at pH 4.5. J. Mol. Biol. *373*, 811–819.

Danty, E., Briand, L., Michard-Vanhee, C., Perez, V., Arnold, G., Gaudemer, O., Huet, D., Huet, J.C., Ouali, C., Masson, C., and Pernollet, J.C. (1999). Cloning and expression of a queen pheromone-binding protein in the honeybee: an olfactory-specific, developmentally regulated protein. J. Neurosci. *19*, 7468–7475.

Du, G.H., and Prestwich, G.D. (1995). Protein-structure encodes the ligand-binding specificity in pheromone binding-proteins. Biochemistry *34*, 8726–8732.

Flecha, F.L.G., and Levi, V. (2003). Determination of the molecular size of BSA by fluorescence anisotropy. Biochem. Mol. Biol. Educ. *31*, 319–322.

Graham, L.A., and Davies, P.L. (2002). The odorant-binding proteins of *Drosophila melanogaster*: annotation and characterization of a divergent gene family. Gene *292*, 43–55.

Grosse-Wilde, E., Gohl, T., Bouche, E., Breer, H., and Krieger, J. (2007). Candidate pheromone receptors provide the basis for the response of distinct antennal neurons to pheromonal compounds. Eur. J. Neurosci. *25*, 2364–2373.

Ha, T.S., and Smith, D.P. (2006). A pheromone receptor mediates 11-cis-vaccenyl acetate-induced responses in *Drosophila*. J. Neurosci. *26*, 8727–8733.

Hansen, K. (1984). Discrimination and production of disparlure enantiomers by the gypsy-moth and the nun moth. Physiol. Entomol. *9*, 9–18.

Honson, N. (2006). Structure and Function of Pheromone-Binding Proteins from the Gypsy Moth, *Lymantria Dispar* (Burnaby, Canada: Simon Fraser University).

Honson, N., Johnson, M.A., Oliver, J.E., Prestwich, G.D., and Plettner, E. (2003). Structure-activity studies with pheromone-binding proteins of the gypsy moth, *Lymantria dispar*. Chem. Senses *28*, 479–489.

Honson, N., Gong, Y., and Plettner, E. (2005). Structure and function of insect odorant and pheromone-binding proteins (OBPs and PBPs) and chemosensory-specific proteins (CSPs). In Chemical Ecology and Phytochemistry of Forest Ecosystems, J.T. Romeo, ed. (Oxford: Elsevier Ltd.), pp. 227–268.

Inkster, J.A.H., Ling, I., Honson, N.S., Jacquet, L., Gries, R., and Plettner, E. (2005). Synthesis of disparlure analogues, using resolution on microcrystalline cellulose triacetate-I. Tetrahedron Asymmetry *16*, 3773–3784.

Isin, E.M., and Guengerich, F.P. (2007). Multiple sequential steps involved in the binding of inhibitors to cytochrome p450 3A4. J. Biol. Chem. *282*, 6863–6874.

Kim, M.S., Repp, A., and Smith, D.P. (1998). LUSH odorant-binding protein mediates chemosensory responses to alcohols in *Drosophila melanogaster*. Genetics *150*, 711–721.

Kowcun, A., Honson, N., and Plettner, E. (2001). Olfaction in the gypsy moth, *Lymantria dispar*: effect of pH, ionic strength, and reductants on pheromone transport by pheromone-binding proteins. J. Biol. Chem. *276*, 44770–44776.

Krieger, J., and Breer, H. (1999). Olfactory reception in invertebrates. Science *286*, 720–723.

Krieger, J., Raming, K., and Breer, H. (1991). Cloning of genomic and complementary-DNA encoding insect pheromone binding-proteins: evidence for microdiversity. Biochim. Biophys. Acta *1088*, 277–284.

Kruse, S.W., Zhao, R., Smith, D.P., and Jones, D.N.M. (2003). Structure of a specific alcohol-binding site defined by the odorant binding protein LUSH from *Drosophila melanogaster*. Nat. Struct. Biol. *10*, 694–700.

Lartigue, A., Gruez, A., Spinelli, S., Riviere, S., Brossut, R., Tegoni, M., and Cambillau, C. (2003). The crystal structure of a cockroach pheromone-binding protein suggests a new ligand binding and release mechanism. J. Biol. Chem. *278*, 30213–30218.

Lartigue, A., Gruez, A., Briand, L., Blon, F., Bezirard, V., Walsh, M., Pernollet, J.C., Tegoni, M., and Cambillau, C. (2004). Sulfur single-wavelength anomalous diffraction crystal structure of a pheromone-binding protein from the honeybee *Apis mellifera* L. J. Biol. Chem. *279*, 4459–4464.

Laughlin, J.D., Ha, T.S., Jones, D.N.M., and Smith, D.P. (2008). Activation of pheromone-sensitive neurons is mediated by conformational activation of pheromone-binding protein. Cell *133*, 1255–1265.

Lautenschlager, C., Leal, W.S., and Clardy, J. (2007). *Bombyx mori* pheromone-binding protein binding nonpheromone ligands: implications for pheromone recognition. Structure *15*, 1148–1154.

Leal, W.S. (2000). Duality monomer-dimer of the pheromone-binding protein from *Bombyx mori*. Biochem. Biophys. Res. Commun. *268*, 521–529.

Leal, W.S., Chen, A.M., Ishida, Y., Chiang, V.P., Erickson, M.L., Morgan, T.I., and Tsuruda, J.M. (2005). Kinetics and molecular properties of pheromone binding and release. Proc. Natl. Acad. Sci. USA *102*, 5386–5391.

Lee, D., Damberger, F.F., Peng, G.H., Horst, R., Guntert, P., Nikonova, L., Leal, W.S., and Wuthrich, K. (2002). NMR structure of the unliganded *Bombyx mori* pheromone-binding protein at physiological pH. FEBS Lett. *531*, 314–318.

Maida, R., Steinbrecht, A., Ziegelberger, G., and Pelosi, P. (1993). The pheromone binding-protein of Bombyx mori: purification, characterization, and immunocytochemical localization. Insect Biochem. Mol. Biol. *23*, 243–253.

Mohanty, S., Zubkov, S., and Gronenborn, A.M. (2004). The solution NMR structure of *Antheraea polyphemus* PBP provides new insight into pheromone recognition by pheromone-binding proteins. J. Mol. Biol. *337*, 443–451.

NagnanLeMeillour, P., Huet, J.C., Maibeche, M., Pernollet, J.C., and Descoins, C. (1996). Purification and characterization of multiple forms of odorant/pheromone binding proteins in the antennae of *Mamestra brassicae* (Noctuidae). Insect Biochem. Mol. Biol. *26*, 59–67.

Pace, C.N., Vajdos, F., Fee, L., Grimsley, G., and Gray, T. (1995). How to measure and predict the molar absorption-coefficient of a protein. Protein Sci. *4*, 2411–2423.

Paduraru, P.A., Popoff, R.T.W., Nair, R., Gries, R., Gries, G., and Plettner, E. (2008). Synthesis of substituted alkoxy benzene minilibraries, for the discovery of new insect olfaction or gustation inhibitors. J. Comb. Chem. *10*, 123–134.

Pesenti, M.E., Spinelli, S., Bezirard, V., Briand, L., Pernollet, J.C., Tegoni, M., and Cambillau, C. (2008). Structural basis of the honey bee PBP pheromone and pH-induced conformational change. J. Mol. Biol. *380*, 158–169.

Plettner, E., Lazar, J., Prestwich, E.G., and Prestwich, G.D. (2000). Discrimination of pheromone enantiomers by two pheromone binding proteins from the gypsy moth *Lymantria dispar*. Biochemistry *39*, 8953–8962.

Sandler, B.H., Nikonova, L., Leal, W.S., and Clardy, J. (2000). Sexual attraction in the silkworm moth: structure of the pheromone-binding-protein-bombykol complex. Chem. Biol. *7*, 143–151.

Steinbrecht, R.A. (1997). Pore structures in insect olfactory sensilla: a review of data and concepts. Int. J. Insect Morphol. Embryol. *26*, 229–245.

Vite, J.P., Klimetzek, D., Loskant, G., Hedden, R., and Mori, K. (1976). Chirality of Insect Pheromones - Response Interruption by Inactive Antipodes. Naturwissenschaften *63*, 582–583.

Vogt, R.G., and Riddiford, L.M. (1981). Pheromone binding and inactivation by moth antennae. Nature *293*, 161–163.

Vogt, R.G., Kohne, A.C., Dubnau, J.T., and Prestwich, G.D. (1989). Expression of pheromone binding-proteins during antennal development in the gypsy-moth *Lymantria dispar*. J. Neurosci. *9*, 3332–3346.

Xu, P.X., Atkinson, R., Jones, D.N.M., and Smith, D.P. (2005). *Drosophila* OBP LUSH is required for activity of pheromone-sensitive neurons. Neuron *45*, 193–200.

Zubkov, S., Gronenborn, A.M., Byeon, I.J.L., and Mohanty, S. (2005). Structural consequences of the pH-induced conformational switch in *A. polyphemus* pheromone-binding protein: mechanisms of ligand release. J. Mol. Biol. *354*, 1081–1090.

